Report

www.the-innovation.org

Shear-flow-induced graphene coating microfibers from microfluidic spinning

Yunru Yu,[1,2] Jiahui Guo,[3] Han Zhang,[3] Xiaocheng Wang,[2] Chaoyu Yang,[2] and Yuanjin Zhao[1,2,3,4,*]

*Correspondence: yjzhao@seu.edu.cn

Received: September 3, 2021; Accepted: January 15, 2022; Published Online: January 19, 2022; https://doi.org/10.1016/j.xinn.2022.100209

GRAPHICAL ABSTRACT

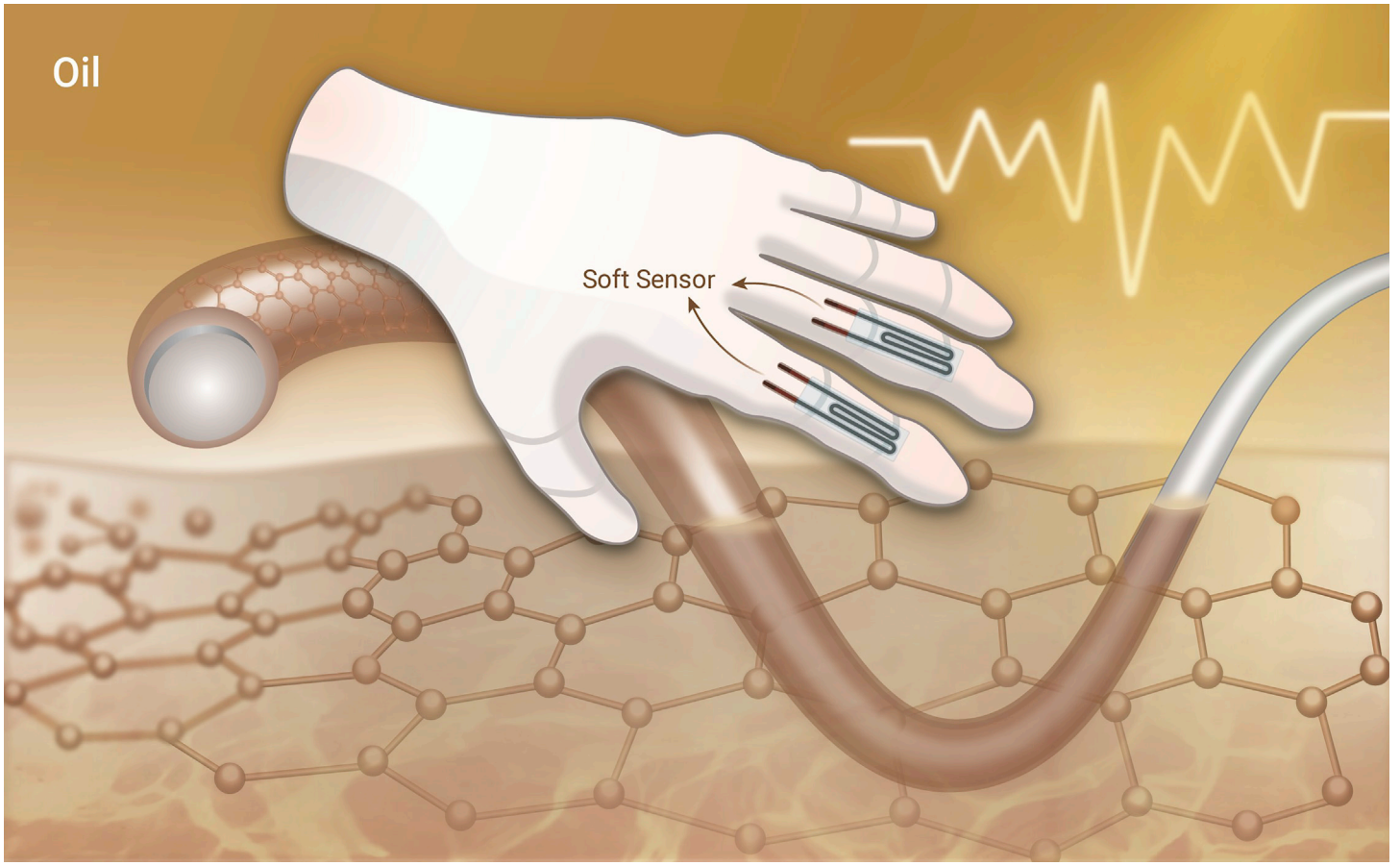

PUBLIC SUMMARY

- Advancements in flexible electronics calls for invention of fiber-based electronic systems by surface modification or encapsulation
- To realize generation and modification of microfibers, shear-flow-induced graphene coating microfibers are obtained from dip coating integrated microfluidics
- The GO coating provided the microfiber with conductivity and thermal responsiveness
- These functional microfibers could be applied as soft sensors and gesture indicators in flexible electronics

Report

Shear-flow-induced graphene coating microfibers from microfluidic spinning

Yunru Yu,[1,2] Jiahui Guo,[3] Han Zhang,[3] Xiaocheng Wang,[2] Chaoyu Yang,[2] and Yuanjin Zhao[1,2,3,4,*]

[1]Department of Clinical Laboratory, The Affiliated Drum Tower Hospital of Nanjing University Medical School, Nanjing 210008, China

[2]Oujiang Laboratory, Zhejiang Lab for Regenerative Medicine, Vision, and Brain Health, Wenzhou Institute, University of Chinese Academy of Sciences, Wenzhou, Zhejiang 325000, China

[3]State Key Laboratory of Bioelectronics, School of Biological Science and Medical Engineering, Southeast University, Nanjing 210096, China

[4]Institute for Stem Cell and Regeneration, Chinese Academy of Science, Beijing 100101, China

*Correspondence: yjzhao@seu.edu.cn

Received: September 3, 2021; Accepted: January 15, 2022; Published Online: January 19, 2022; https://doi.org/10.1016/j.xinn.2022.100209

Citation: Yu Y., Guo J., Zhang H., et al., (2022). Shear-flow-induced graphene coating microfibers from microfluidic spinning. The Innovation **3(2)**, 100209.

The advancements in flexible electronics call for invention of fiber-based electronic systems by surface modification or encapsulation. Here we present novel shear-flow-induced graphene nanosheets coating microfibers by integrating the dip coating approach with the microfluidic spinning method. The core hydrogel microfiber was first spun continuously from the microfluidic device, and the shear flow from the dip coating approach allowed formation of the thin graphene oxide (GO) nanosheet coating shell. Because the fluid components and flow rates in the microfluidic spinning together with the lifting speed in the dip coating approach are highly controllable, the morphology of the resultant microfibers could be precisely tailored, including the core-shell structure, conductivity, and thermal responsibilities. These features equipped the resultant microfibers with the potential of thermal and motion sensors, and their value in gesture indicators has also been explored. Microfibers generated from such a simple and controllable method could be versatile in flexible electronics.

INTRODUCTION

Functional fibrous materials have attracted a lot of attention over the paste several decades and hold great promise, especially with advances in flexible electronics.[1–4] A myriad of smart systems constructed from designable and versatile fibers are receiving extensive research interest and reveal superior sensing,[5] energy harvesting,[6,7] actuation,[8] and many other properties.[9,10] These fibers could be imparted with electronic functions on the surface through surface modification or inside the fibers via encapsulation of electronically functioning organic or inorganic reagents.[11–13] The development of nanotechnology facilitates processing of nanomaterials on flexible fiber substrates.[14–18] Through direct coating methods, transferring approaches, and printing or drawing patterns, metal nanowires, metal oxide nanorods, carbon nanotubes, conductive polymers, and graphene have been integrated into fiber-based flexible electronic systems.[19–22] Despite the tremendous progress that has been made, practical application of the fiber and fiber-based electronics is challenging because of weak control over the uniformity of the applied nanomaterials. In addition, although cost-effective and large-scale fabrication techniques have been realized, preparation of major functional fibers is still restricted by complicated step-by-step modifications or physiochemical reactions. Therefore, inspiring approaches to generating functional fibers with comparatively uniform functional structures in a feasible and controllable manner are highly anticipated.

In this paper, we present novel shear-flow-induced graphene nanosheets coating microfibers by using a microfluidic spinning method, as shown in Figure 1. The microfluidics technique is regarded as a promising method for preparation of functional materials because of its mature flow control ability.[23–26] In the world of microfluidics, the behavior of flow streams is considerably different from those at the macro scale because of the effect of surface forces that play important roles at the micro level but are often neglected at the macro scale. The shear force that exists at the interface of two immiscible flows with rate differences results in diversified styles of droplets as well as microfibers.[27–30] In addition, the wettability of the microfluidic channels and the generated materials affects the flow dynamics and nanoparticle assemblies by controlling their action routes in the microchannel.[31,32] However, recent approaches to microfluidics have not been applied to generate microfibers with nanomaterial-encapsulated shells, and their value for soft and flexible electronics remain to be investigated.

Here we present a dip coating integrated microfluidic spinning method for continuous microfiber generation and graphene oxide (GO) nanosheet coating (Figure 1). During the fabrication process, the core hydrogel microfiber forms when the central sodium alginate liquid flow merges with the sheath calcium chloride solution. The GO nanosheet homogeneous shell is deposited when the formed hydrogel microfiber flows into and lifts out of the coating pool which contains layered silicon oil and GO nanosheet-dispersed sodium alginate solution. Benefitting from the shear force caused by the fast lifting of the hydrogel together with the rapid gelation process of the alginate hydrogel, the GO nanosheets can be coated at the surface of the core microfiber and fixed within the sheath hydrogel shell. Because these processes can be tuned by adjusting the flow rates and lifting speed, the diameter of the core microfiber, the shell thickness, as well as the conductivity of the core-shell microfiber are controllable. In addition, the concentration of GO nanosheet dispersion affects the surface characteristics, thermal responsiveness, and conductivity of the resultant microfibers. Potential use of these microfibers in flexible electronics, including soft sensors and gesture indicators, has also been explored. All of these features demonstrate that the shear-flow-induced GO coating microfiber based on microfluidic spinning is simple to prepare and versatile in flexible electronics.

RESULTS AND DISCUSSION

In a typical experiment, the inner sodium alginate (SA) solution flowed along the inner tapered capillary. The calcium chloride solution was pumped into the device from the interval between the square and collection capillaries as the sheath flow (Figure S1A). Because of the centrosymmetric construction of the capillary microfluidic device, a 3D co-flow formed when SA was jetted into the collection channel. With the coaxial stream flowing, the fast calcium ion diffusion at the interface of the two miscible flows resulted in cross-linking of calcium alginate (CA) hydrogel. As a result, a CA microfiber could be spun continuously and collected in the CA gelation bath, which was the core microfiber for further dip coating (Figures S1B and 2A). Benefitting from the manipulation of flow rates during microfluidic spinning, the diameter of such a cylindrical microfiber could be easily adjusted by tuning the central SA flow rate or the sheath calcium chloride flow rate (Figures S1C and S1D). Although, in this study, the range of the fiber diameter is around 150–500 μm, it could be adjusted by changing the microfluidic parameters. The relationship between the microfiber diameter and the flow rate showed that an increase in the central flow rate or a decrease in the sheath flow rate brought about an increase in diameter, whereas an increased sheath flow rate or a reduced central flow rate resulted in a decrease in diameter.

Because the fast ion crosslinking between calcium ions and SA chains would prevent the GO-dispersed SA solution from coating, the formed core hydrogel microfiber underwent a washing process before it ran into the coating bath. The dip coating process took place based on the different wettabilities of the layered silicone oil, GO nanosheet-dispersed SA solution, and the hydrogel microfiber. When the microfiber was lifted from the coating bath, a thin layer was formed at the interface of the silicone oil and CA microfiber, which provided a hydrophilic surface for superspreading of GO nanosheets dispersion. The lifting manner provided a strong shear flow between the GO nanosheet dispersion and the hydrogel microfiber, allowing formation of a thin layer containing GO nanosheets that covered the core microfiber (Figure 2B). The shear-flow-induced GO-coating microfiber was then generated continuously and collected in the shell gelation bath, where fast crosslinking of the SA in the coating layer took place, and the GO nanosheets could be encapsulated (Figure 2C). Because of the uniform cylindrical structure of the hydrogel microfiber and the straight lifting process, the layer was thin and homogeneous under a bright-field microscope.

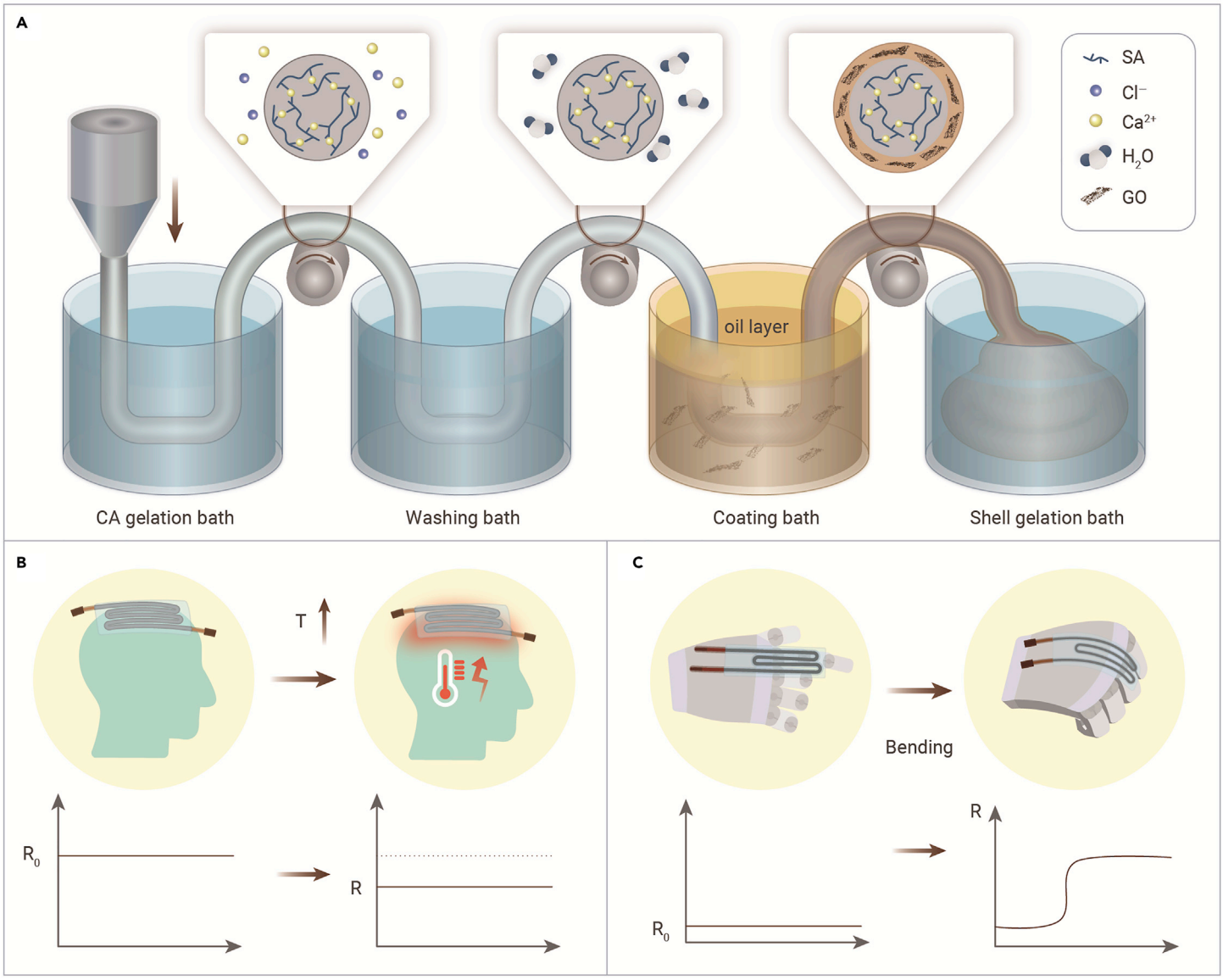

Figure 1. Schematics of the generation and application of the shear-flow-induced GO-coating microfiber (A) Microfluidic spinning and dip coating processes of the microfiber. The CA gelation bath contained calcium chloride solution, the washing bath contained deionized water, the coating bath was filled with layered silicone oil and SA dispersed with GO nanosheet solution, and the shell gelation bath was a calcium chloride solution. (B) The microfiber-integrated flexible film is used as a thermal sensor. (C) The microfiber-integrated flexible film responds to deformation.

To make it clear, fluorescent nanoparticles were introduced into the GO nanosheet-dispersed SA solution to fabricate the microfiber.The resulting GO nanosheet-coating microfiber was characterized by confocal laser-scanning microscopy. The images showed that the coating layer was thin and well covered the central hydrogel microfiber (Figures 2D and S2A). The morphology of such a microfiber would also be affected by the concentration of the GO nanosheets dispersed in the SA solution. With increasing concentration, the microfiber showed a darker color under a stereoscopic microscope (Figures S2B–S2F). The customizable lifting speed, which can be controlled by the rotating speed of the wheel that transports the microfiber, provides the microfiber with a tunable coating thickness ranging from about 10–80 μm (Figure S3). The accelerated lifting speed dramatically reduced the shell thickness; as a result, by further increasing the lifting speed, a microfiber with an ultra-thin coating layer where GO nanosheets quasi-2D aligned could be achieved.

The scanning electron microscopic (SEM) images of the cross-section and the shell margin of the prepared microfiber also showed the core-shell structure of the microfiber and the existence of GO nanosheets in the microfiber shell (Figures 2E and 2F). The core and shell of the microfiber separated because of the different compositions, resulting in different shrinking degrees during sample preparation. Apart from the SEM images, transmission electron microscopy and Raman spectra also indicated the existence of GO nanosheets in the microfiber shell. They showed that GO nanosheets were successfully encapsulated in the microfiber, which kept the same morphology in the dispersion (Figure S4). Also, the GO nanosheet-coating microfiber appeared two characteristic peaks, the same as the GO sample in Raman spectra, whereas the pure CA hydrogel microfiber did not (Figure S5A). This revealed the presence of GO in the microfiber. In addition, the intensity of the characteristic peaks of GO depicted the GO concentration in the microfiber shell. These results suggested that the incremental concentration of coating GO nanosheets exhibited stronger characteristic peak intensities, which provided the microfiber with enhanced surface characteristics (Figure S5B). This demonstrated that, by taking advantage of the easily tuned microfluidic spinning and dip-coating processes, the core-shell structure, GO encapsulation, and surface characteristics of the microfiber could be customized.

As a commonly used graphene-based material, the GO nanosheets encapsulated in the shell provide the microfiber with basic conductivity. The resistance of the core-shell-structured microfibers with different lengths and dispersion concentrations was investigated. According to the statistical results, the resistance increased when the length of the microfiber increased, and it decreased when the concentration of GO dispersion increased (Figures 3A and 3B). These results strictly complied with the law of resistance ($R = \rho L/S$), where ρ refers to the

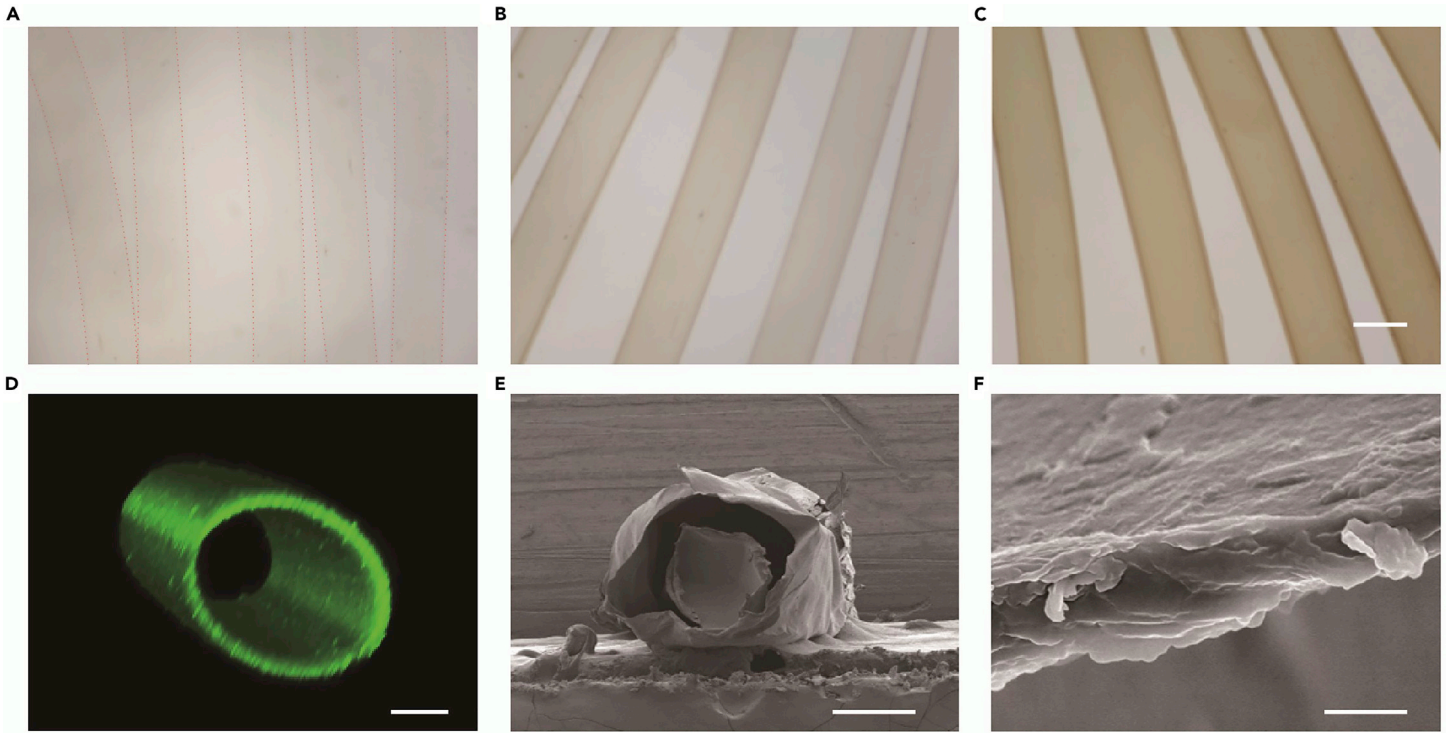

Figure 2. Characterization of microfibers (A) Bright-field microscopy image of the core hydrogel microfibers. (B) Stereomicroscopy image of the microfiber after coating the GO nanosheet dispersion. (C) Microscopy photograph of the generated shear-flow-induced GO nanosheet-coating microfiber. (D) 3D reconstruction of confocal laser-scanning microscopy images of the coating microfiber. (E) SEM image of the cross-section of the microfiber. (F) Detailed SEM image of the graphene nanosheets on the microfiber shell. Scale bars represent (C) 350 μm, (D) 250 μm, (E) 250 μm, and (F) 2 μm.

resistivity of the sheath hydrogel containing GO nanosheets, L is the length of the microfiber, and S is the area of the microfiber sheath. With increasing encapsulation of GO nanosheets in the microfiber shell, the conductivity of the hybrid hydrogel enhanced so that the resistivity of the microfiber is reduced, resulting in a decrease in microfiber resistance. When stretching these microfibers, their resistance also responds to the elongation because of the distribution of GO

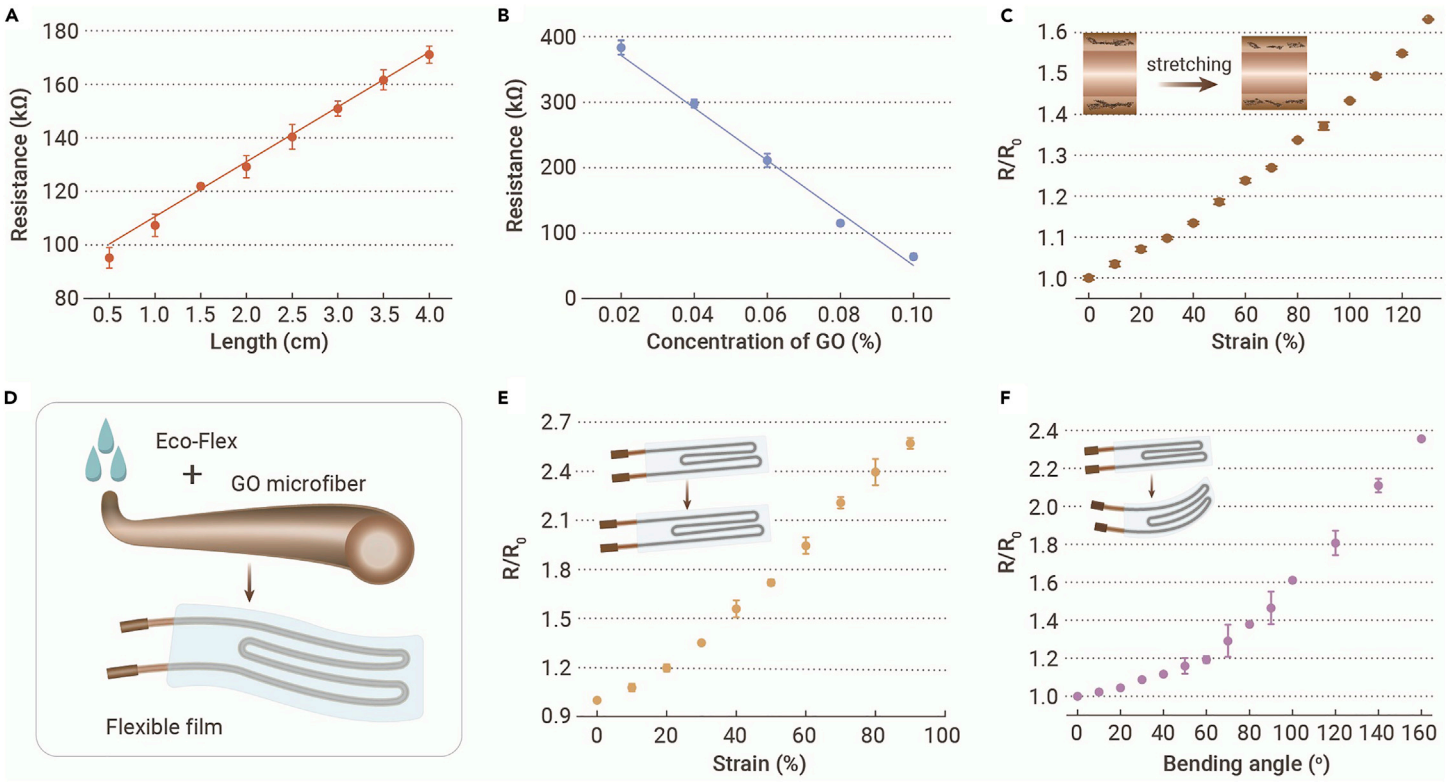

Figure 3. Conductive performance of the microfiber and the microfiber-integrated flexible film (A) The resistance of microfibers of different lengths. (B) The relationship between the resistance of the microfiber and the concentration of GO nanosheets in the dispersion solution. (C) The relative resistance of the microfiber during stretching. (D) Schematic of the generation of the microfiber-integrated flexible film. (E) Relative resistance of the flexible film when stretched. (F) Different resistance values of the microfiber-integrated film during the bending process.

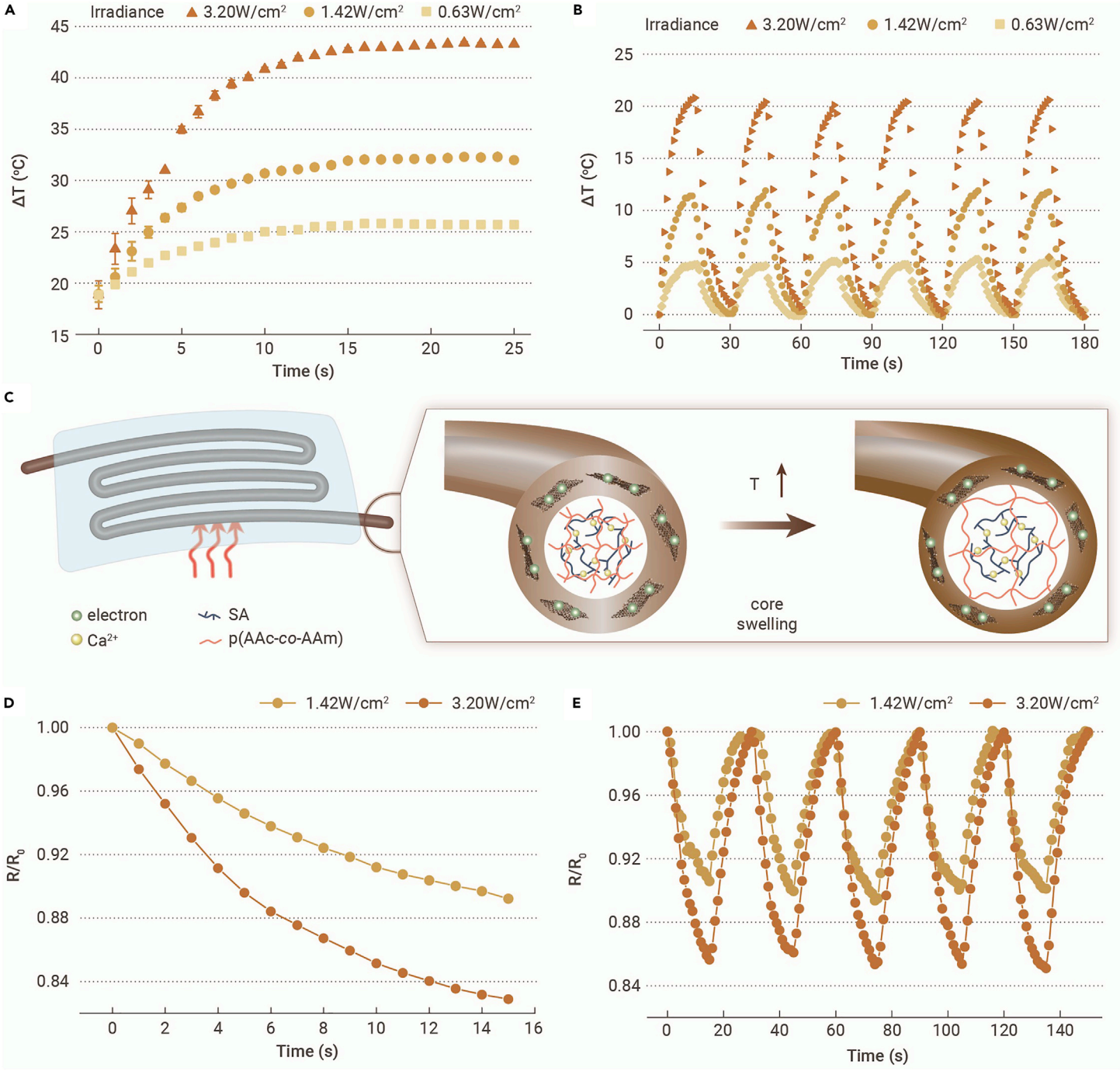

Figure 4. Thermal responsiveness of the microfiber (A) Photothermal reaction of the microfiber under irradiation of 0.63, 1.42, and 3.20 W/cm^2. (B) Temperature changes of the microfiber during cyclic photothermal heating and natural cooling with different irradiance. (C) Schematic showing the microstructure of the graphene-coating microfiber during the heating period. (D) Relative resistance of the microfiber-integrated flexible film exposed to NIR irradiation of 1.42 and 3.20 W/cm^2. (E) Cyclic relative resistance changes of the flexible film in five heating and cooling cycles.

nanosheets. Before stretching the microfiber, the stress-strain response of the microfiber was tested (Figure S6). The curve described that the pure CA microfiber could be stretched to around 240%, whereas the GO-coating microfiber broke its shell at around 160% of strain and finally ruptured at around 240%. This could be attributed to avoidance of mechanical degradation resulting from misalignment of the GO nanosheets. During the stretching process, its relative resistance (R/R_0, where R is the resistance in real time and R_0 is the original resistance) were recorded (Figure 3C). The resistance arrived at a 60% increase when the microfiber was stretched to 130% of its original length. This increase may be attributed to the extension of the gap between GO nanosheets that are trapped in the coating layer.

The value of these GO nanosheet coating microfibers can be realized by encapsulating them in a stretchable film because the conductive GO coating is easily damaged, and the hydrogel dehydrates during deformation. By using transparent Eco-flex as the elastic base and the fabricated microfiberas the conductive medium, the flexible film was easily achieved (Figures 3D and S7). The resistance of this flexible conductive film was recorded during deformation. The relative resistance increased remarkably to over 2 times its original resistance when stretching the flexible film to almost 2 times its original length, indicating a sensitive response to the stretching (Figure 3E). This could also be attributed to the increase in the electron paths from the increased distance between conductive GO nanosheets. Its stability after cycled stretching was also studied (Figure S8). The relative resistance increased slightly after hundreds of cycles, which may result from slow dehydration during the stretching period. When bent to certain degrees, the flexible film showed corresponding increased resistance because the bending also caused an increase in nanosheet distance

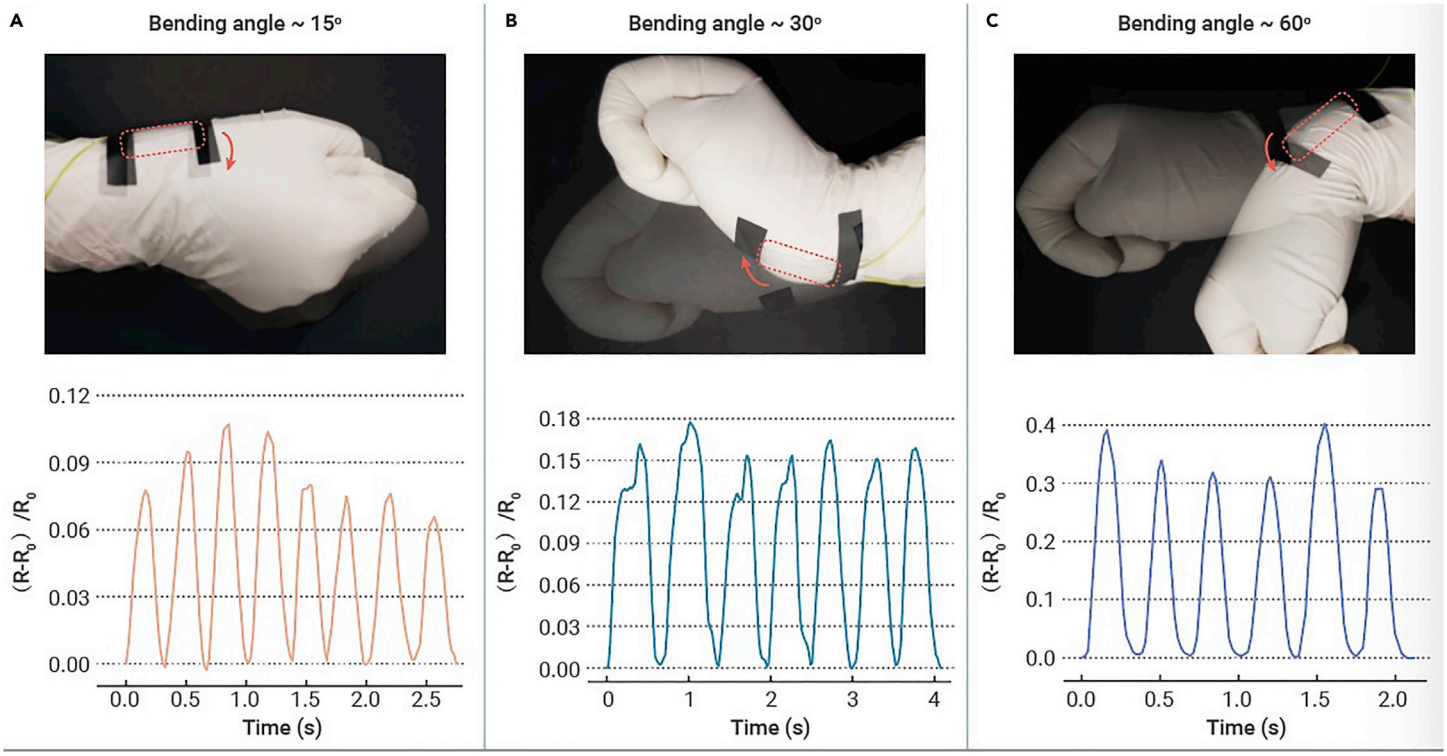

Figure 5. Microfiber-integrated flexible film applied as a joint motion sensor (A–C) Real-time images of the flexible film stuck on different parts of the elbow when bent. (D–E) Relative resistance changes with the elbow bending at different angles.

(Figure 3F). These features make the flexible film integrated with a graphene coating microfiber a candidate for flexible sensors.

The GO nanosheets encapsulated in the microfiber shell also provide the microfiber with photothermal responsiveness. The responsive behavior of the microfiber under the near-infrared (NIR) irradiation was investigated by weaving the microfiber into a plate. It could be inferred that GO coating played an important part in the photothermal responsiveness of the microfiber via the contrast experiment (Figure S9A). During this period, the temperature of the plate at different time intervals was recorded (Figure 4A). It was found that exposure to NIR light of 3.20 W/cm^2 raised the central temperature of the microfiber plate to around 40°C within 15 s, and the highest temperature stabilized around 43°C. This rapid thermal response remained when the radiation intensity was reduced to 1.42 and 0.63 W/cm^2, and the final temperatures were around 30 and 25°C, respectively. In addition, microfibers coated with different concentrations of GO nanosheets showed different temperature changes under the same strength of NIR light (Figure S9B). This shows that the increased concentration caused the increased temperature, which may be attributed to the accumulated photothermal transfer. Apart from such responses, the microfiber also showed repeated heating and cooling cycles activated by the repeatedly working NIR light (Figure 4B). In each cycle, which lasted about 30 s, the microfiber plate heated up to its highest temperature in the first 15 s when the NIR light was switched on and cooled down to its original temperature when the light was off at a relatively low room temperature, which created a cycled temperature change. This temperature change could be tuned by applying different irradiation intensities and would not be affected after encapsulation into the transparent flexible film. When the microfiber plate was exposed to a cycled NIR light of 3.20 W/cm^2, the temperature change reached about 20°C, whereas it reduced to around 11°C and 5°C when exposed to the radiation of 1.42 and 0.63 W/cm^2, respectively.

By using thermally responsive hydrogel as the core microfiber, the photothermal response of the graphene-coating microfiber could be converted to the resistance changing ability. To achieve a thermal responsive core, acrylamide (AAm) and acrylic acid (AAc) were added to the SA solution and polymerized under UV illumination to form a double-network hydrogel (Figure 4C). When the microfiber was exposed to NIR radiation, the photothermal ability of GO nanosheets enabled an increase in the temperature of the microfiber, including the core hydrogel. When the temperature increases, the water molecules redistribute in the sheath layer and the core hydrogel because the hydrogen bonds between pAAc (poly(acrylic acid)) and pAAm (polyacrylamide) chains dissociated, as a result, p(AAc-*co*-AAm) absorbed the water in the shell hydrogel. This caused shrinking of the graphene coating layer so that the distances between each nanosheet were greatly reduced. Together with the intensified interior electron motion in the increased temperature, the resistance of the microfiber decreased greatly, and the decline was consistent with the irradiation (Figure 4D). Because the water redistribution was reversible, the resistance response behavior of the microfiber also showed repeatability when exposed to cycled irradiation, as shown in Figure 4E. For a 30-s cycle of irradiation and natural cooldown, the resistance of the microfiber showed a sharp decline followed by a quick rise. These relative resistance did not deteriorate after five cycles, showing stable thermally conductive sensing ability. Specifically, under irradiation of 1.42 W/cm^2, the resistance of the microfiber decreased to 90% of its initial level and could recover within 15 s. When irradiation increased to 3.20 W/cm^2, the relative reduction of its resistance increased to 15%. These results showed that the resulting microfiber had potential as a negative temperature coefficient thermistor in a thermal sensing system.

Apart from the thermal sensing ability, the flexible film could be applied as a motion sensor and gesture indicator because of its flexibility. The obtained GO microfibers were treated with hydroiodic acid for the reduction process, after which the conductive performance of the microfiber was enhanced. To explore this practical value, the real-time relative resistance change was recorded when the film was stuck to the elbow (Figures 5A–5C). The relative resistance changed with the bending motion of the elbow, and the amplitude of the changes indicated different bending angles according to the resistance change curves (Figures 5D–5F). In addition, when attaching the flexible film to the finger, it could depict the finger bending and pressing activities (Figures S10 and S11). The increase in bending range and the pressing force caused a dramatic increase in the resistance change of the flexible film, indicating its potential as a motion and touch sensor when used as electronic skin.

Moreover, the motion-sensing ability of the flexible film contributes to its application as a gesture indicator. By fixing flexible films to the finger joints, the resistance of the films would change according to different sign languages. In this case, different bending and straightening combinations of the thumb,

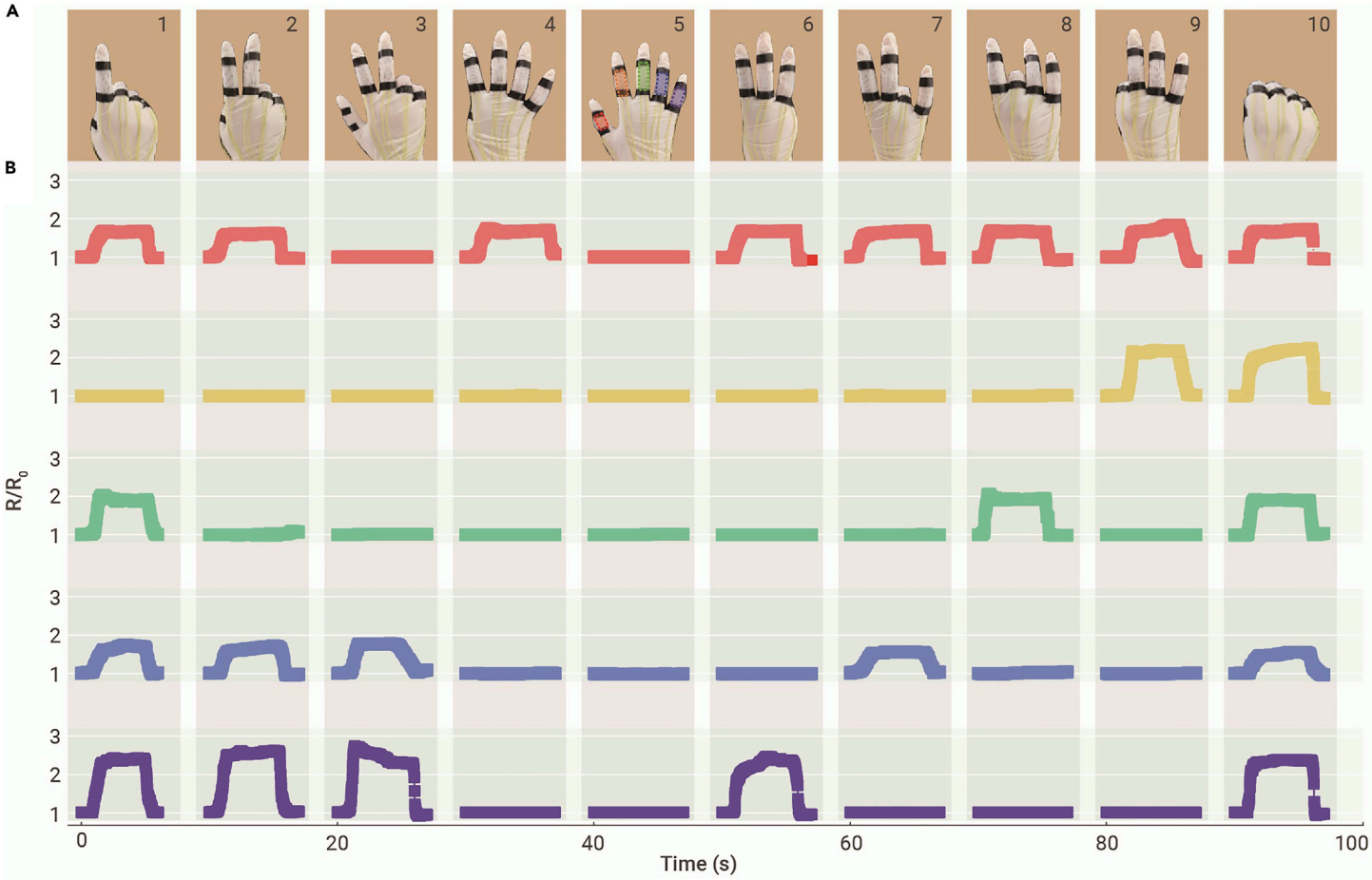

Figure 6. The microfiber-integrated flexible film used as a gesture indicator (A) Digital photographs of the films fixed on fingers showing different numbers. (B) Relative resistance change curves of the films fixed on different fingers.

index, middle, ring, and little finger are executed to indicate different numbers (Figure 6A). As shown in Figure 6B, the resistance of flexible films corresponding to each finger quickly responded to the gestures and experienced increases and decreases. Because the bending angles of each finger were different when they represented different numbers, the relative resistance changes were slightly different. As a result, varied gestures could be interpreted by analyzing the relative resistance change curves. All of this showed that the microfiber-integrated flexible films had the capability of real-time gesture monitoring and indicating.

CONCLUSIONS

In conclusion, we propose a shear-flow-induced graphene-coating microfiber from a dip coating-integrated microfluidic spinning technique. The hydrogel core of the microfiber can be continuously obtained from simple and controllable microfluidic spinning. The coating of GO nanosheets was facilitated by superspreading of the GO nanosheet dispersion on the hydrogel microfiber coming from different wettabilities of the hydrogel microfiber and silicone oil, together with the shear flow resulting from the fast lifting process in the coating bath. The conductive and photothermal response ability of the graphene coating layer endowed the microfiber with conductivity and thermal response performance. Especially, the thermally responsive core hydrogel caused an obvious resistance change of the microfiber, showing its potential as a thermal sensor. In addition, we applied the microfiber-integrated flexible films as motion sensors and gesture indicators. The immediate reaction and sensitive resistance changes demonstrated the value of these hybrid films in the flexible sensing field. Such shear-flow-induced graphene-coating microfibers fabricated from simple and controllable microfluidic spinning is versatile in flexible electronics applications.

Taking advantage of the manipulation of flow rates in microfluidic spinning and lifting speed in the dip coating procedure, morphologies like core diameter and shell thickness of the graphene-coating microfiber are highly controllable. Thus, we believe that, by further optimizing the dip coating method, an ultra-thin layer of quasi-2D nanosheet alignment could be achieved. In addition, the thermal response and sensing performances could be adjusted by changing the dispersion concentration of GO nanosheets during dip coating. It is also possible that other kinds of nanomaterials, including MXenes and black phosphorus nanosheets,[33,34] could be coated on the microfibers via this dip coating-integrated microfluidic spinning method. Such kinds of microfibers would find practical applications in the electronics, optics, or biomedical fields.

MATERIALS AND METHODS

Materials

SA and AAm (Analytical Reagent, 99.0%) were from Aladdin. Calcium chloride, AAc, N, N-methylene-bisacrylamide (Bis), and the photoinitiator 2-hydroxy-2-methyl1-phenyl-1-propanone (HMPP) were obtained from Sigma-Aldrich. GO nanosheet dispersion (1 mg/mL) was purchased from XFNano. The flexible base Eco-flex 00-30 was bought from Smooth-On and used as received. Deionized water was obtained from a Millipore Milli-Q water purification system and kept its resistivity at 18.2 MΩ cm. Before microfluidic spinning, all of the solutions were prepared and filtered.

Microfluidic preparation of the hydrogel core microfiber

A coaxial capillary microfluidic device was used for continuous spinning of the core microfiber. To achieve this, capillaries with outer and inner diameters of 1.0 mm and 750 μm (World Precision Instruments) were used. The inner capillary was pulled and sanded to the desired orifice before using, and the outer capillary was used as received. The inner and outer capillaries were then coaxially arranged in a square capillary with an inner diameter of 1.05 mm (AIT Glass) for observation. A transparent epoxy resin was used to stabilize and seal the capillaries where necessary. For microfiber spinning, the inner phase of SA was 2 wt %, and the calcium chloride solution flowing in the sheath and contained in the CA gelation bath was 2 wt %. For thermally responsive hydrogel microfiber spinning, the inner flow was a mixture of 2 wt % SA, 5 wt % AAm, 5 wt % AAc, 0.5 wt % Bis, and

1% HMPP, and the sheath flow was still the 2 wt % calcium chloride solution. After it was formed *in situ* in the collection channel and collected in the CA gelation bath, the microfiber was exposed to UV illumination for crosslinking of p(AAm-*co*-AAc). For the reduced GO-coating microfiber, the obtained GO-coating microfiber was treated with hydroiodic acid (40%, 80°C) for more than 12 h.[35]

Dip coating of GO nanosheets on the hydrogel microfiber

The hydrogel microfiber was first rinsed with water in the cleaning bath before it was immersed in the coating bath to remove the remaining calcium ions, which would affect uniform formation of the coating layer. After cleansing, the microfiber was immersed in the coating bath, which contained layered silicone oil and GO nanosheet-dispersed SA solution, and lifted straight. To achieve different GO concentrations, GO nanosheet dispersion and SA solution were mixed at different ratios to achieve a final SA concentration of 1 wt % and GO concentrations of 0.01%, 0.02%, 0.04%, 0.06%, 0.08%, and 0.10%. The lifting speed of the microfiber could be adjusted by adjusting the rotation speed of the wheel.

The coating layer was polymerized after immersion and collection of the microfiber in the shell gelation bath.

Fabrication of microfiber-integrated flexible films

By applying the Eco-flex precursors to the prepared graphene-coating microfiber and polymerizing the flexible substrate, a flexible film could be fabricated. The resultant graphene-coating microfiber was first washed to remove the oil on its surface and stabilized on the plate in a designed pattern. Then the two Eco-flex precursors were mixed thoroughly, poured onto the microfiber, and solidified to form a hybrid film at room temperature.

Conductivity tests of the microfibers and flexible films

Different resistance and real-time resistance changes of the graphene-coating microfibers and microfiber-integrated flexible films were recorded using a traditional two-probe technique on a digital multimeter (Keithley, DMM6500). A vernier caliper and a protractor were used to indicate the strain and bending of the testing examples. To avoid unnecessary interference, silver glue was used at the connection joints between the material and the testing probes. The flexible film was attached to the gloves by using an adhesive tape, and the volunteer wore the gloves and moved in the sensing applications. All experiments were carried out in compliance with the relevant laws and with the approval of the Scientific Ethical Committee of Oujiang Laboratory (Zhejiang Lab for Regenerative Medicine, Vision and Brain Health), Wenzhou Institute, University of Chinese Academy of Sciences.

Thermal responsiveness of the microfiber

The resultant microfiber was first arranged as a plate to receive relatively uniform NIR irradiation (808-nm laser system, Xilong Laser). Various laser power densities (0.63, 1.42, and 3.20 W/cm^2) were applied to the microfiber plate. The temperature change was continuously monitored by a thermal imaging system (FILR, E5) and recorded every second. The photothermal stability of the microfiber was tested for 5 cycles, and the real-time relative resistance was recorded at the same time by connecting the microfiber to the digital multimeter.

Characterization

Real-time microfluidic spinning was monitored by a fast camera (Pike, F032B). Bright-field microscopy photographs were obtained using a stereomicroscope (Jiangnan Novel Optics, JSZ6S) equipped with an industrial digital camera (Cossim). SEM images were taken using a field emission SEM (Hitachi, SU8010), and transmission electron microscopy photos were taken using a field emission transmission electron microscope (FEI, Talos). The Raman spectra of the materials were obtained using a laser microconfocal Raman spectrometer (Renishaw, inVia). The stiffness test of the microfibers was carried out on an electronic universal testing machine (Instron, 5944). The digital images of the flexible films stabilized on the joints and fingers were taken using a digital camera.

REFERENCES

1. Liu, Z., Fang, S., Moura, F., et al. (2015). Hierarchically buckled sheath-core fibers for superelastic electronics, sensors, and muscles. Science ***349***, 400–404.
2. Wang, L., Wang, L., Zhang, Y., et al. (2018). Weaving sensing fibers into electrochemical fabric for real-time health monitoring. Adv. Funct. Mater. ***28***, 1804456.
3. Zeng, W., Shu, L., Li, Q., et al. (2014). Fiber-based wearable electronics: a review of materials, fabrication, devices, and applications. Adv. Mater. ***26***, 5310–5336.
4. Ding, T., Chan, K.H., Zhou, Y., et al. (2020). Scalable thermoelectric fibers for multifunctional textile-electronics. Nat. Commun. ***11***, 1–8.
5. Wang, L., Xie, S., Wang, Z., et al. (2020). Functionalized helical fibre bundles of carbon nanotubes as electrochemical sensors for long-term in vivo monitoring of multiple disease biomarkers. Nat. Biomed. Eng. ***4***, 159–171.
6. Tao, X. (2019). Study of fiber-based wearable energy systems. Acc. Chem. Res. ***52***, 307–315.
7. Guo, J., Yu, Y., Zhang, D., et al. (2021). Morphological hydrogel microfibers with MXene encapsulation for electronic skin. Research (Wash D. C.) ***2021***, 7065907.
8. Wang, C., Sim, K., Chen, J., et al. (2018). Soft ultrathin electronics innervated adaptive fully soft robots. Adv. Mater. ***30***, 1706695.
9. Shao, F., Hu, N., Su, Y., et al. (2020). Non-woven fabric electrodes based on graphene-based fibers for areal-energy-dense flexible solid-state supercapacitors. Chem. Eng. J. ***392***, 123692.
10. Wen, Z., Yeh, M.-H., Guo, H., et al. (2016). Self-powered textile for wearable electronics by hybridizing fiber-shaped nanogenerators, solar cells, and supercapacitors. Sci. Adv. ***2***, e1600097.
11. Xu, T., Zhang, Z., and Qu, L. (2020). Graphene-based fibers: recent advances in preparation and application. Adv. Mater. ***32***, 1901979.
12. Yu, Y., Guo, J., Sun, L., et al. (2019). Microfluidic generation of microsprings with ionic liquid encapsulation for flexible electronics. Research (Wash D. C.) ***2019***, 6906275.
13. Zhang, P., Zhao, C., Zhao, T., et al. (2019). Recent advances in bioinspired gel surfaces with superwettability and special adhesion. Adv. Sci. ***6***, 1900996.
14. Wan, S., Chen, Y., Fang, S., et al. (2021). High-strength scalable graphene sheets by freezing stretch-induced alignment. Nat. Mater. ***20***, 624–631.
15. Kim, Y.H., Kim, D.J., Lee, S., et al. (2019). Microfluidic designing microgels containing highly concentrated gold nanoparticles for SERS analysis of complex fluids. Small ***15***, 1905076.
16. Fang, R., Liu, M., and Jiang, L. (2020). Design of nanoparticle systems by controllable assembly and temporal/spatial regulation. Adv. Funct. Mater. ***30***, 1903351.
17. Liu, W., Zhao, L., Wang, C., and Zhou, J. (2020). Conductive nanomaterials for cardiac tissues engineering. Engineered Regen. ***1***, 88–94.
18. Guo, C.F., and Ding, L. (2021). Integration of soft electronics and biotissues. The Innovation (N. Y.) ***2***, 100074. https://doi.org/10.1016/j.xinn.2020.100074.
19. Zhao, C., Zhang, P., Zhou, J., et al. (2020). Layered nanocomposites by shear-flow-induced alignment of nanosheets. Nature ***580***, 210–215.
20. Chen, Y., Deng, Z., Ouyang, R., et al. (2021). 3D printed stretchable smart fibers and textiles for self-powered e-skin. Nano Energy ***84***, 105866.
21. Sim, K., Chen, S., Li, Z., et al. (2019). Three-dimensional curvy electronics created using conformal additive stamp printing. Nat. Electron. ***2***, 471–479.
22. Zhang, Y.-L., Li, J.-C., Zhou, H., et al. (2021). Electro-responsive actuators based on graphene. The Innovation (N. Y.) ***2***, 100168. https://doi.org/10.1016/j.xinn.2021.100168.
23. Miri, A.K., Nieto, D., Iglesias, L., et al. (2018). Microfluidics-enabled multimaterial maskless stereolithographic bioprinting. Adv. Mater. ***30***, 1800242.
24. Nam, S.K., Kim, J.B., Han, S.H., and Kim, S.-H. (2020). Photonic Janus balls with controlled magnetic moment and density asymmetry. ACS Nano ***14***, 15714–15722.
25. Zhang, J., Zeng, L., Qiao, Z., et al. (2020). Functionalizing double-network hydrogels for applications in remote actuation and in low-temperature strain sensing. ACS Appl. Mater. Inter. ***12***, 30247–30258.
26. Shao, C., Liu, Y., Chi, J., et al. (2019). Responsive inverse opal scaffolds with biomimetic enrichment capability for cell culture. Research (Wash D. C.) ***2019***, 9783793.
27. Lee, T.Y., Lee, S., Kim, Y.H., et al. (2019). Microfluidic fabrication of capsule sensor platform with double-shell structure. Adv. Funct. Mater. ***29***, 1902670.
28. Chen, G., Yu, Y., Wu, X., et al. (2019). Microfluidic electrospray niacin metal-organic frameworks encapsulated microcapsules for wound healing. Research (Wash. D. C.) ***2019***, 6175398.
29. Lashkaripour, A., Rodriguez, C., Mehdipour, N., et al. (2021). Machine learning enables design automation of microfluidic flow-focusing droplet generation. Nat. Commun. ***12***, 1–14.
30. Yu, Y., Guo, J., Ma, B., et al. (2020). Liquid metal-integrated ultra-elastic conductive microfibers from microfluidics for wearable electronics. Sci. Bull. ***65***, 1752–1759.
31. Liu, J., Yu, L.J., Yue, G., et al. (2019). Thermoresponsive graphene membranes with reversible gating regularity for smart fluid control. Adv. Funct. Mater. ***29***, 1808501.
32. Du, X.Y., Li, Q., Wu, G., and Chen, S. (2019). Multifunctional micro/nanoscale fibers based on microfluidic spinning technology. Adv. Mater. ***31***, 1903733.
33. Zheng, Y., Yin, R., Zhao, Y., et al. (2021). Conductive MXene/cotton fabric based pressure sensor with both high sensitivity and wide sensing range for human motion detection and E-skin. Chem. Eng. J. ***420***, 127720.
34. Shen, X.F., Song, L.L., and Zhang, L.S. (2018). Preparation of TiO2/C3N4 heterojunctions on carbon-fiber cloth as efficient filter-membrane-shaped photocatalyst for removing various pollutants from the flowing wastewater. J. Colloid Interf. Sci. ***532***, 798–807.
35. Kuila, T., Mishra, A.K., and Lee, J.H. (2013). Recent advances in the efficient reduction of graphene oxide and its application as energy storage electrode materials. Nanoscale ***5***, 52–71.

ACKNOWLEDGMENTS

This work was supported by the National Key Research and Development Program of China (2020YFA0908200), the Strategic Priority Research Program of the Chinese Academy of Science (XDA16021103), the National Natural Science Foundation of China (52073060 and 61927805), the Shenzhen Fundamental Research Program (JCYJ20190813152616459 and JCYJ20210324133214038), the China Postdoctoral Science Foundation (2020M680652), and the Natural Science Foundation of Zhejiang Province of China (LQ22E030004).

AUTHOR CONTRIBUTIONS

Y.Zhao conceived the idea and designed the experiments. Y.Yu carried out the experiments. Y.Yu and Y.Zhao analyzed data and wrote the paper. J.Guo, H.Zhang, X.Wang, and C.Yang contributed to scientific discussions of the article.

DECLARATION OF INTERESTS

The authors declare no competing interests.

LEAD CONTACT WEBSITE

www.zhaoyuanjin.com.

SUPPLEMENTAL INFORMATION

Supplemental information can be found online at https://doi.org/10.1016/j.xinn.2022.100209.